The European Journal of Research and Development

journals.orclever.com/ejrnd

OR CLEVER Science & Research Group

Research Article

Preamble-Based Symbol Timing Algorithms in OFDM Systems

Kemal Yağlı[1*], Sultan Aldırmaz Çolak[2*]

[1] Kocaeli University, Faculty of Engineering, Department of Electronics and Communication, Kocaeli, Turkey, (ORCID: 0000-0002-9986-9659), kemalyagli07@gmail.com

[2] Kocaeli University, Faculty of Engineering, Department of Electronics and Communication, Kocaeli, Turkey, (ORCID: 0000-0001-7154-0723), sultan.aldirmaz@kocaeli.edu.tr

[*] Correspondence: kemalyagli07@gmail.com; Tel.: (+905547854858)

(First received February 05, 2022 and in final form June 04, 2022)

Reference: Yağlı, K., & Aldırmaz Çolak, S. Preamble-Based Symbol Timing Algorithms in OFDM Systems. *The European Journal of Research and Development*, *2*(2), 445–458.

Abstract

In orthogonal frequency division multiplexing (OFDM) systems, a preamble is added at the start of the OFDM data frame in order to find the correct frame starting point. In the receiver, the symbol starting point is estimated by a correlation-based timing metric that uses the periodic properties of the preamble. In this study, a novel preamble structure using the constant amplitude zero autocorrelation (CAZAC) sequence is proposed. The performance of the timing synchronization algorithms has been compared with the proposed method in terms of mean squared error (MSE). The simulations are performed under additive white Gaussian noise (AWGN) and Rayleigh multipath fading channels. The simulation results indicate that our proposed method provides better timing MSE performance for the low signal-to-noise ratio (SNR) values.

Keywords: Orthogonal frequency division multiplexing (OFDM), Preamble, Constant amplitude zero autocorrelation (CAZAC) sequence, Synchronization, Timing.

1. Introduction

Orthogonal frequency division multiplexing (OFDM) is widely used in many wireless communication applications such as wireless fidelity (Wi-Fi), long-term evolution (LTE), and LTE-Advanced (LTE-A) standards as well as fifth generation (5G) systems due to its high spectral efficiency and broadband structure. However, it is quite sensitive to symbol timing and carrier frequency offset that destroy the orthogonality among subcarriers. These impairments cause inter-symbol interference (ISI) and inter-

carrier interference (ICI). Therefore, synchronization in the OFDM receiver is one major step that must be carried out [1].

The synchronization step in OFDM systems is divided into two groups as time and frequency synchronization. The aim of OFDM timing synchronization is to estimate the correct symbol starting point at which the fast Fourier transform (FFT) will be performed in the receiver. Besides, frequency synchronization is needed to correct the distortions in frequency that may occur due to Doppler shift or phase differences between local oscillators [2]. There are several studies in which time and frequency synchronization are both analyzed together and separately [3-6].

For timing synchronization, the periodic structure contained in time domain signal is used. There is a periodic structure in the nature of the OFDM systems. To eliminate the ISI effect caused by multipath propagation, cyclic prefix (CP) is used. CP is generated by repeating the last a few samples of the OFDM symbol. CP length should be chosen longer than the maximum delay spread of the channel in order to avoid ISI. In studies where additional structures are not used, the correlation of the CP is generally employed [7,8]. However, the performance of these methods is lower than the preamble-based algorithms which are used in most communication standards.

The most popular algorithm is proposed by Schmidl & Cox in which the autocorrelation of the preamble structure with two identical halves is used [1]. Although it is a simple and robust method, the timing metric creates an undesired plateau effect. The plateau effect is defined as a peak throughout all CP samples. This effect causes uncertainty at the start of the OFDM frame. Minn et al. reduced this plateau effect by using negative samples in the preamble structure [9]. However, their algorithm produces side lobes around the symbol starting point. Later, Park et al. and Kim et al. desired to obtain sharper symbol timing estimation by reducing the side lobes [10,11]. For preamble structure, Ren et al. used a constant amplitude zero autocorrelation (CAZAC) sequence [12].

CAZAC sequence is exploited due to its ideal correlation properties in many applications such as channel estimation and synchronization [13-15]. One of the CAZAC type sequence, Zadoff-Chu sequence, is used in LTE and LTE-A standards. For downlink synchronization, the Zadoff-Chu sequence is used in the primary synchronization signal (PSS). The user equipment (UE) estimates the slot timing and physical layer identity with PSS. During the cell search procedure, the base station (eNodeB) sends the PSS by selecting one of the 3 different parameter values of the Zadoff-Chu sequence. The UE estimates the selected parameter value by using the correlation function between the local copies of 3 PSS signals and the received signal. Thus, one of the 3 physical layer identities is estimated in addition to timing synchronization [16].

Moreover, Zadoff-Chu sequences with different parameter values and cyclically-shifted versions of these sequences are used for synchronization in the uplink physical

random access channel (PRACH) in LTE and LTE-A systems. The UE requests access to the eNodeB over PRACH by transmitting a random access preamble. The uplink transmission timing of the UE and the eNodeB is synchronized by sending the random access preamble [17].

In this study, different timing algorithms are analyzed in detail and a new preamble structure that takes advantage of the ideal correlation properties of the CAZAC sequence is proposed.

The rest of the paper is organized as follows. In Section 2, preliminary information on timing synchronization algorithms for OFDM systems is given. CAZAC sequence is introduced in Section 3. Section 4 describes the proposed preamble structure. In Section 5, simulation results are presented and discussed. And finally, in Section 6 the conclusion is given.

2. Preliminary Information on Timing Synchronization Algorithms for OFDM Systems

In OFDM, bits are modulated with desired modulation schemes in frequency domain and each symbol is assigned to different and orthogonal subcarriers. Then, inverse FFT (IFFT) is taken over N subcarriers. To prevent the channel-induced ISI effect CP is added. Thus, the OFDM frame is constituted.

OFDM timing synchronization is needed to estimate the correct symbol starting point. At the receiver, FFT will be performed for each OFDM symbol in the frame. The presence of samples from the previous or next OFDM symbol in the FFT window causes inaccurate demodulation. The ISI free region, in which the symbol starting point should be estimated in order to maintain the orthogonality among subcarriers is illustrated in Figure 1. If the estimated symbol starting point is in the CP samples that are not interfered by the multipath channel delay propagation, the orthogonality among the subcarriers is not destroyed.

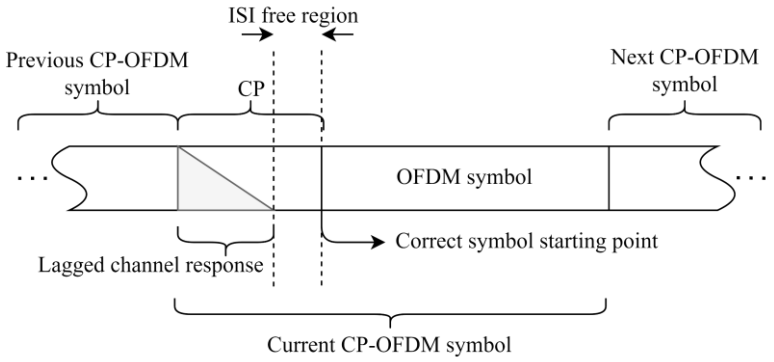

Figure 1 ISI free region for symbol timing estimation [18].

The effect of the symbol timing error in ISI free region can be observed by taking the N-point FFT of the estimated OFDM symbol. Samples of the estimated OFDM symbol in the time domain can be written as $\{x[n+\delta]\}_{n=0}^{N-1}$. N denotes the number of subcarriers. With the FFT process, samples in the frequency domain can be given as $X[k]e^{j2\pi k\delta/N}$ where δ is symbol timing error and k is subcarrier index, k = 0, 1, …, N-1. This causes a phase offset that is proportional to δ and k rotating the signal constellation diagram around the origin. This effect is compensated by the channel equalization in the receiver [2]. Periodically extending the OFDM symbol using CP can prevent the symbol timing error only in ISI free region. For this reason, it is necessary to estimate the symbol starting point with high accuracy.

For timing synchronization, a preamble structure is placed in front of the frame in the transmitter. In the receiver, a timing metric is used to estimate the symbol starting point by analyzing the preamble structure. The general form of the timing metric is as follows:

$$M_x(d) = \frac{|P_x(d)|^2}{\left(R_x(d)\right)^2}, \tag{1}$$

where x denotes the method's name, i.e. x = {Schmidl, Minn, Park, Kim, Ren}. $P_x(d)$ analyzes the correlation of the corresponding samples within the preamble structure and $R_x(d)$ is used for the normalization of the timing metric by defining the energy of the received signal. Indexes of the received signal's samples are shown with d. $P_x(d)$ and $R_x(d)$ differ according to each method. In the following subsections, correlation-based timing algorithms, which are frequently used in the literature, are introduced.

2.1.Schmidl's Method

The symbol timing estimation is provided by the preamble with two identical halves in the time domain [1]. The samples of the preamble are as follows:

$$S_{Schmidl} = [A_{N/2} \;\; A_{N/2}], \tag{2}$$

where $A_{N/2}$ represents a random complex-valued pseudo-noise (PN) sequence of length $N/2$. N denotes the length of the preamble vector used, as well as the FFT size. $P_{Schmidl}(d)$, which analyzes the correlation of the corresponding samples within the $N/2$ length window and $R_{Schmidl}(d)$, which is used for the normalization of the timing metric by defining the energy of the received signal, are given in Equation (3) and Equation (4).

$$P_{Schmidl}(d) = \sum_{k=0}^{N/2-1} r^*(d+k)r\left(d+k+\frac{N}{2}\right), \tag{3}$$

$$R_{Schmidl}(d) = \sum_{k=0}^{N/2-1} \left| r\left(d + k + \frac{N}{2}\right) \right|^2, \quad (4)$$

where $(.)^*$ denotes the complex conjugate operation and $r(n)$ represents n-th sample of the received signal. The complex conjugate of a sample in the first half is multiplied by the sample in the second half. Since the corresponding pairs within the preamble samples will have the same phase and amplitude under no channel distortion, the sum of their products reaches the maximum value. Therefore, the index of the start point (first sample) of the preamble is estimated by $\arg\max_d M_{Schmidl}(d)$ where $M_{Schmidl}(d)$ is the timing metric computed according to Equation (1). Then, by adding N and CP length (G) to the estimated index, the estimated symbol starting point ($\widehat{d}$) is obtained.

As can be seen from Equation (3), the difference between $P_{Schmidl}(d)$ and $P_{Schmidl}(d+1)$ is small. Because the sum of the products expressed as $r^*(d+1)\, r(d+1+N/2) + r^*(d+2)\, r(d+2+N/2) + \cdots + r^*(d+N/2-1)\, r(d+N-1)$ between two consecutive samples is the same. Only the products of $r^*(d)\, r(d+N/2)$ and $r^*(d+N/2)\, r(d+N)$ differ [12]. Moreover, the timing metric produces a plateau effect giving a peak across all CP samples used for the preamble. This effect leads to uncertainty for the symbol timing estimation.

2.2.Minn's Method

The preamble in Minn's method is to reduce the uncertainty caused by the previous method [9]. The time domain preamble structure is updated as follows:

$$S_{Minn} = [A_{N/4} \quad A_{N/4} \quad -A_{N/4} \quad -A_{N/4}], \quad (5)$$

where $A_{N/4}$ shows a PN sequence of length $N/4$. Correlation and energy equations are given in Equation (6) and Equation (7), respectively.

$$P_{Minn}(d) = \sum_{m=0}^{1} \sum_{k=0}^{N/4-1} r^*\left(d + \frac{N}{2}m + k\right) r\left(d + \frac{N}{2}m + k + \frac{N}{4}\right), \quad (6)$$

$$R_{Minn}(d) = \sum_{m=0}^{1} \sum_{k=0}^{N/4-1} \left| r\left(d + \frac{N}{2}m + k + \frac{N}{4}\right) \right|^2. \quad (7)$$

In the timing metric, the index of the preamble's first sample is estimated by $\arg\max_d M_{Minn}(d)$. After that, $\hat{d}$ is obtained by adding N and G to the estimated index. As

a consequence of the negative-valued samples in the preamble, the peak is obtained only for the symbol starting point.

2.3.Park's Method

Unlike Minn's method, $A_{N/4}$ and its symmetric version in the time domain ($B_{N/4}$) are used together in Park's method [10]. The form of the time domain preamble, correlation and energy equations are given in Equation (8), Equation (9), and Equation (10), respectively.

$$S_{Park} = [A_{N/4} \quad B_{N/4} \quad A_{N/4}{}^{*} \quad B_{N/4}{}^{*}], \tag{8}$$

$$P_{Park}(d) = \sum_{k=0}^{N/2} r(d-k)r(d+k), \tag{9}$$

$$R_{Park}(d) = \sum_{k=0}^{N/2} |r(d+k)|^2. \tag{10}$$

The index of the first sample of the second half is estimated by $\arg\max_{d} M_{Park}(d)$. Unlike other methods $\hat{d}$ is obtained by adding *N/2* and *G* to the estimated index. $P_{Park}(d)$ is designed to have *N/2* different pairs of products for two consecutive d values. Namely, there is one common product for every two consecutive d values. Therefore, with Park's metric, an impulse-shaped peak is obtained only at the symbol starting point under no channel distortion. It is desired to obtain high performance by reducing the side lobes around the symbol starting point formed in Minn's method.

2.4.Kim's Method

In Kim's method, similar to Park's method, it is aimed to increase the difference between the pairs of products calculated for consecutive samples [11]. The preamble structure is given with updated correlation and energy equations as follows:

$$S_{Kim} = [A_{N/4} \quad B_{N/4}{}^{*} \quad A_{N/4} \quad B_{N/4}{}^{*}], \tag{11}$$

$$P_{Kim}(d) = \sum_{k=0}^{N/2-1} r\left(d-k+\frac{N}{2}\right) r\left(d+k+\frac{N}{2}\right), \tag{12}$$

$$R_{Kim}(d) = \sum_{k=0}^{N/2-1} \left| r\left(d + k + \frac{N}{2}\right) \right|^2. \quad (13)$$

When the metric calculation is performed with $P_{Kim}(d)$, there are $N/2$ different pairs of products between two consecutive d samples. In the timing metric, the index of the preamble's first sample is estimated by $\arg\max_d M_{Kim}(d)$. Then, similar to the first two methods mentioned, $\hat{d}$ is obtained.

2.5.Ren's Method

In Ren's method, an algorithm is proposed similar to Schmidl's method. Alternatively, a CAZAC sequence is used for the preamble structure. In addition, the preamble is sent by being weighted with an N-length PN sequence randomly formed from +1 and -1 values at the transmitter [12]. The preamble structure has used by Ren's method is in the following form:

$$S_{Ren} = [C_{N/2} \quad C_{N/2}] o \, S_N, \quad (14)$$

where $C_{N/2}$ represents the CAZAC sequence with $N/2$ samples. S_N denotes PN sequence of length N. Moreover, o represents the Hadamard product operator between vectors. Correlation and energy equations are given in Equation (15) and Equation (16).

$$P_{Ren}(d) = \sum_{k=0}^{N/2-1} s_k s_{k+N/2} r^*(d+k)\, r\left(d + k + \frac{N}{2}\right), \quad (15)$$

$$R_{Ren}(d) = \frac{1}{2} \sum_{k=0}^{N-1} |r(d+k)|^2. \quad (16)$$

Similar to Park and Kim's methods, the symbol starting point is estimated in an impulse shape by increasing the difference between pairs of products. The PN sequence used in the transmitter is known by the receiver. Accordingly, during the metric calculation performed by the receiver, the weighting of the preamble samples at the transmitter is eliminated by multiplying with $s_k s_{k+N/2}$. In the timing metric, the index of the first sample of the preamble is estimated by $\arg\max_d M_{Ren}(d)$. Similar to other methods except for Park's method, $\hat{d}$ is obtained.

In order to visualize symbol timing estimation methods, we simulated them for the preamble length N=256 and CP length G=32 under no channel distortion. The simulation results are given in Figure 2. The correct symbol starting point is indexed to 0. In Schmidl's method, the plateau effect can be seen easily. For all CP samples, the output of

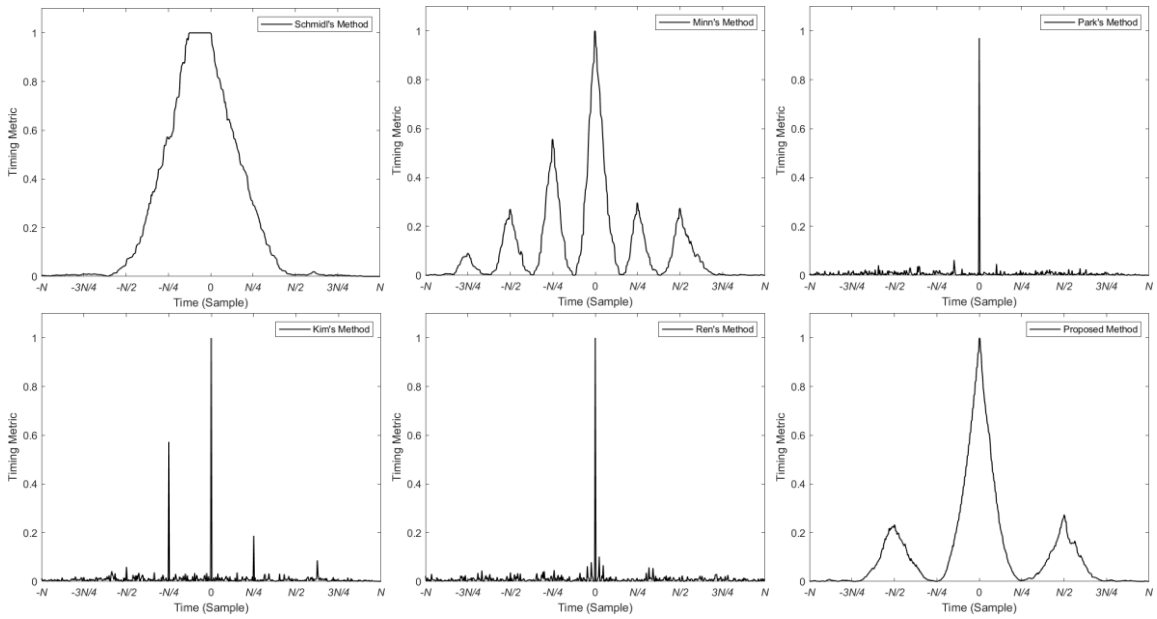

Figure 2 Symbol timing estimation methods under no channel distortion (N=256, G=32).

timing metric is equal to 1. While Park, Kim, and Ren's methods obtain impulse-shaped timing metrics, Minn's method gives many undesired minor peaks which are reduced by the proposed method (it will be introduced in Section 4).

3. CAZAC Sequence

CAZAC sequence is used to increase the performance of timing algorithms since it has ideal properties [19]. CAZAC complex exponential sequence, which is a kind of polyphase code, and its autocorrelation function are given in Equation (17) and Equation (18).

$$c(n) = e^{j\pi\mu n^2/N_p}, \qquad 0 \le n \le N_p - 1 \tag{17}$$

$$\sum_{n=0}^{N_p-1} c(n)c^*(n+\tau) = \begin{cases} N_p & ,\tau = 0 \\ 0 & ,\tau \neq 0 \end{cases}. \tag{18}$$

N_p is the period of the sequence, μ is a parameter that specifies the root sequence that can be generated depending on the period of the sequence. τ represents the number of cyclic shifts. In order to satisfy Equation (18), μ must be chosen to be relatively prime to N_p [20]. If N_p is chosen as a prime number, $N_p - 1$ root sequences can be generated. Therefore, the number of root sequences that can be generated is limited. In other words, for a CAZAC sequence with a period of N_p, it is possible to generate root sequences equal to the number of relatively prime integers to N_p. Other sequences can be generated by cyclically shifted versions of the root sequence.

CAZAC sequence has better correlation properties than that of PN sequences. The normalized autocorrelation graph of the CAZAC and PN sequences is given in Figure 3. As can be seen from the figure, the autocorrelation between the root sequence and its cyclically shifted version yields zero.

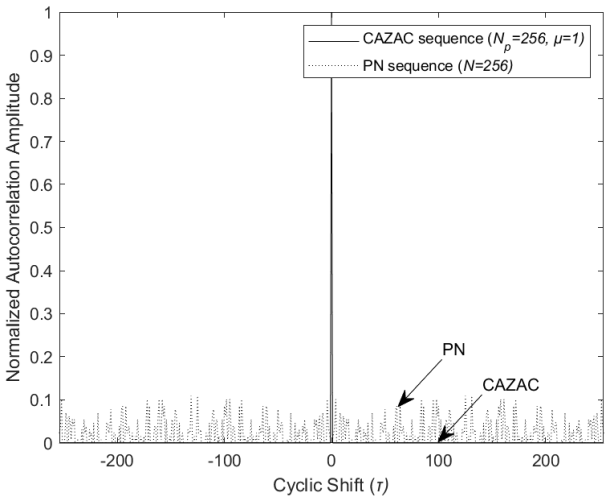

Figure 3 Autocorrelation of the CAZAC and PN sequences.

Furthermore, the properties of the CAZAC sequence do not change as a result of IFFT or FFT. Therefore, unlike the PN sequence, it has a constant amplitude in both time and frequency domains. Hence, it provides a low peak to average power ratio (PAPR) [20].

4. Proposed Method

Minn et al. suggested a sharper timing algorithm that eliminates the plateau effect as a result of correlation with negative-valued samples in the second half. Despite the elimination of the plateau effect of the timing metric, the form of the side lobes is observed around the symbol starting point. Therefore, in order to improve the performance of symbol timing estimation a new preamble structure is proposed, which prevents the two side lobes in $\hat{d} - N/4$ and $\hat{d} + N/4$ samples. CAZAC sequence is used instead of PN sequence in the structure of the proposed preamble. The samples of the preamble in the time domain are as follows:

$$S_{Proposed} = \left[C_{N/4} \;\; C_{N/4} \;\; C_{\tau_{N/4}} \;\; C_{\tau_{N/4}}\right] \tag{20}$$

where $C_{N/4}$ represents the CAZAC sequence with $N/4$ samples, which can be generated by using Equation (17). $C_{\tau_{N/4}}$ denotes τ sample cyclically shifted version of root sequence. For the cyclic shift, $\tau = N/8$ samples are used in the proposed method. $M_{Minn}(d)$ is used

as the timing metric. By utilizing the zero autocorrelation property of the CAZAC sequence, the similarity between the first half and the second half of the preamble is reduced. As a result of this process, the form of the side lobes in $\hat{d} - N/4$ and $\hat{d} + N/4$ samples are prevented.

In Minn's method, the amplitude of the side lobe that formed in the $\hat{d} - N/4$ is related to the CP length used. When the CP length is taken as $N/4$, another peak occurs in the $\hat{d} - N/4$ as shown in Figure 4. Similar to Schmidl's method, this causes uncertainty for the symbol timing estimation. This effect is also eliminated by the proposed preamble structure.

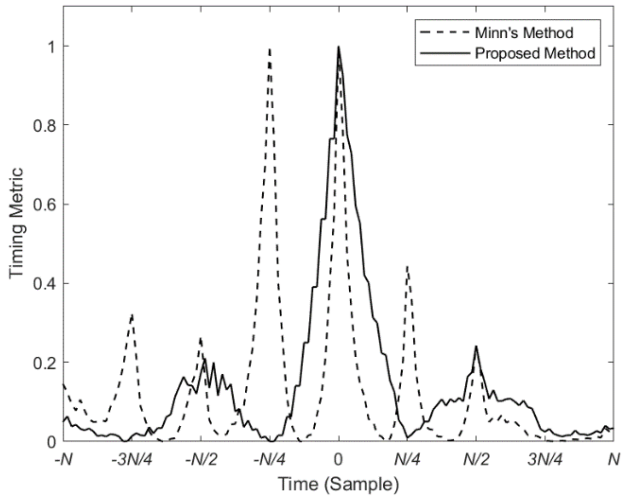

Figure 4 Elimination of the peak formed at the start of the CP (N=64, G=16).

5. Simulation Results

The symbol starting point estimation performance of the symbol synchronization methods in the literature and the proposed method has been evaluated in terms of mean squared error (MSE). Binary phase-shift keying (BPSK) is used for the modulation of subcarriers in OFDM symbols. In the generation of CAZAC sequence, μ is selected as 1. The frame structure used in the simulations is given in Figure 5. Timing metrics are observed for the $2N$ samples around the first sample of the preamble. Simulations are performed both under additive white Gaussian noise (AWGN) and 10-tap Rayleigh multipath fading channel (L=10 paths). The channel paths are modeled with an exponentially decaying power delay profile having average power of $e^{-\ell/L}$, $\ell = 0,1,\ldots,L-1$ [21].

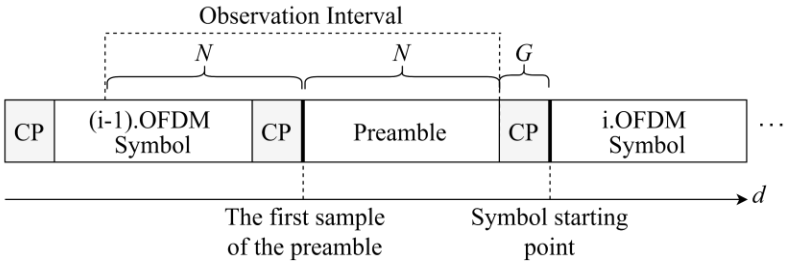

Figure 5 Illustration of the OFDM frame structure used in simulation.

The MSE of estimators is derived as $MSE = \frac{1}{m}\sum_{i=1}^{m}(d_i - \hat{d}_i)^2$ with the correct symbol starting point (d_i) and estimated symbol starting points ($\hat{d}_i$) over the m=10000 independent Monte-Carlo iterations. Signal-to-noise ratio (SNR) is described as the total signal (all the subcarriers) to noise power ratio.

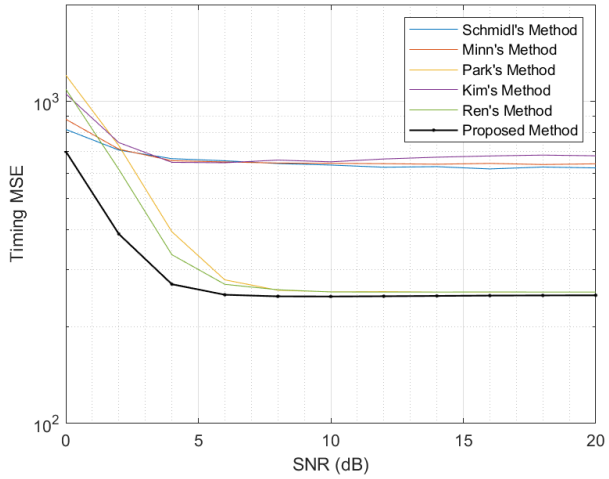

Figure 6 MSE comparison of the methods in the AWGN channel (N=64, G=16).

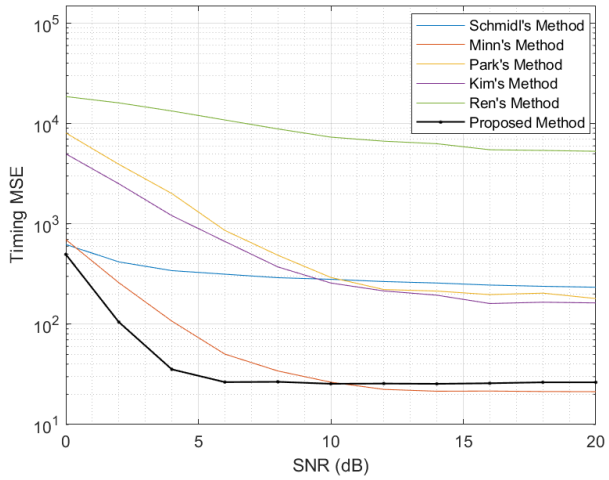

Figure 7 MSE comparison of the methods in the Rayleigh multipath fading channel (N=256, G=32).

In Figure 6 and Figure 7, MSE curves are given in the AWGN channel and Rayleigh multipath fading channel. The plateau effect in Schmidl's method reduces the MSE performance by affecting the symbol timing estimation in both channel conditions. In the case where G is chosen as $N/4$, Minn and Kim's methods create two peak values causing uncertainty in the symbol timing estimation, similar to Schmidl's plateau effect. As shown in Figure 6, it is observed that this effect reduces MSE performance. Due to the fact that Ren and Park propose impulse-shaped timing metric, MSE performance in the AWGN channel increases. However, accuracy degrades in the Rayleigh multipath fading channel. In the simulation conditions, it has been shown that in the AWGN channel and Rayleigh multipath fading channel (when $SNR < 10dB$), the MSE performance of the proposed method is better than the other timing algorithms analyzed.

6. Conclusion

A new preamble is designed for symbol timing estimation. It utilizes the zero autocorrelation property between CAZAC sequence and its cyclically shifted version. The simulation results show that the proposed preamble-based method provides lowest MSE value for low SNR values. Thus, we think that this method can be used for symbol timing in OFDM systems by increasing the performance compared to other timing algorithms.

References

[1] T. M. Schmidl & D. C. Cox (1997). Robust Frequency and Timing Synchronization for OFDM. IEEE Transactions on Communications, vol. 45, no. 12, pp. 1613–1621.

[2] Y.S. Cho, J. Kim, W.Y. Yang & C.G. Kang (2010). MIMO-OFDM Wireless Communications with MATLAB. John Wiley & Sons.

[3] A.B. Awoseyila, C. Kasparis & B.G. Evans (2009). Robust Time-Domain Timing and Frequency Synchronization for OFDM Systems. IEEE Trans. on Consumer Electronics, vol. 55, no. 2, pp. 391-399.

[4] X. Fan, J. Yang & W. Zhang (2020). Time-Frequency Synchronization Design of OFDM Systems Based on CAZAC Sequence. 2020 International Conference on Communications, Information System and Computer Engineering (CISCE), pp. 55-58.

[5] Y.H. Cho & D.J. Park (2013). Timing Estimation Based on Statistical Change of Symmetric Correlator for OFDM System. IEEE Communications Letters, vol. 17, no. 2, pp. 397- 400.

[6] D. Jian, H. Wu, W. Gao & R. Jiang (2018). A Novel Timing Synchronization Method Based on CAZAC Sequence for OFDM Systems. 2018 IEEE International Conference on Signal Processing, Communications and Computing (ICSPCC), pp. 1-5.

[7] J. J. van de Beek, M. Sandell & P. O. Borjesson (1997). ML Estimation of Time and Frequency Offset in OFDM Systems. IEEE Transactions on Signal Processing, vol. 45, no. 7, pp. 1800-1805.

[8] Y. A. Jung, S. B. Byun, H. J. Shin, D. C. Han, S. H. Cho & S. H. Lee (2021). Frequency and Symbol Timing Offset Estimation Method for CP-OFDM Based System. 2021 International Conference on Information and Communication Technology Convergence (ICTC), pp. 599-601.

[9] H. Minn, V. K. Bhargava & K. B. Letaief (2003). A Robust Timing and Frequency Synchronization for OFDM Systems. IEEE Transactions on Wireless Communications, vol. 2, no. 4, pp. 822-839.

[10] B. Park, H. Cheon, C. Kang & D. Hong (2003). A Novel Timing Estimation Method for OFDM Systems. IEEE Communications Letters, vol. 7, no. 5, pp. 239-241.

[11] J. J. Kim, J. H. Noh & K. H. Chang (2005). Robust Timing & Frequency Synchronization Techniques for OFDM-FDMA Systems. IEEE Workshop on Signal Processing Systems Design and Implementation, pp. 716-719.

[12] G. Ren, Y. Chang, H. Zhang & H. Zhang (2005). Synchronization Method Based on a New Constant Envelop Preamble for OFDM Systems. IEEE Transactions on Broadcasting, vol. 51, no. 1, pp. 139-143.

[13] G. Gong, F. Huo & Y. Yang (2013). Large Zero Autocorrelation Zones of Golay Sequences and Their Applications. IEEE Transactions on Communications, vol. 61, no. 9, pp. 3967-3979.

[14] W. Chung, C. Kim, S. Choi & D. Hong (2016). Synchronization Sequence Design for FBMC/OQAM Systems. IEEE Transactions on Wireless Communications, vol. 15, no. 10, pp. 7199-7211.

[15] F. Wu, P. Guo, A. Yang & Y. Qiao (2019). Chromatic Dispersion Estimation Based on CAZAC Sequence for Optical Fiber Communication Systems. IEEE Access, vol. 7, pp. 139388-139393.

[16] Z. Zhang, J. Liu & K. Long (2012). Low-Complexity Cell Search With Fast PSS Identification in LTE. IEEE Transactions on Vehicular Technology, vol. 61, no. 4, pp. 1719-1729.

[17] J. Mišić, V. B. Mišić & N. Khan (2017). Sharing It My Way: Efficient M2M Access in LTE/LTE-A Networks. IEEE Transactions on Vehicular Technology, vol. 66, no. 1, pp. 696-709.

[18] M. M. U. Gul, S. Lee & X. Ma (2012). Robust synchronization for OFDM employing Zadoff-Chu sequence. 2012 46th Annual Conference on Information Sciences and Systems (CISS), pp. 1-6.

[19] M. M. U. Gul, X. Ma & S. Lee (2015). Timing and Frequency Synchronization for OFDM Downlink Transmissions Using Zadoff-Chu Sequences. IEEE Transactions on Wireless Communications, vol. 14, no. 3, pp. 1716-1729.

[20] Z. Yang, L. Dai, J. Wang, J. Wang & Z. Wang (2011). Transmit Diversity for TDS-OFDM Broadcasting System Over Doubly Selective Fading Channels. IEEE Trans. on Broadcasting, vol. 57, no. 1, pp. 135-142.

[21] M. Morelli, C.-C.J. Kuo, & M.-O. Pun (2007). Synchronization Techniques for Orthogonal Frequency Division Multiple Access (OFDMA): A Tutorial Review. Proc. IEEE, vol. 95, no. 7, pp. 1394-1427.